Theoretical study of the double Compton effect with twisted photons

J. A. Sherwin*
Department of Physics, Metropolitan Community College, Omaha, Nebraska 68103-0777, USA
(Received 25 January 2017; published 2 May 2017)

Double Compton scattering of high-energy twisted photons is investigated within the framework of relativistic quantum electrodynamics. We investigate the dependence of the angular distributions of the scattered photons on the parameters of the incident photon beam, such as momentum cone opening angle and projection of orbital angular momentum. Numerical calculations of the angular distributions of the scattered photons are presented for incoming twisted photons and compared to the standard case of incident plane-wave photons. The dependence of the angular distributions of the double-Compton-scattered photons for initially twisted photons prepared in a superposition of two vortex states is also presented.

DOI: 10.1103/PhysRevA.95.052101

I. INTRODUCTION

Among the most fundamental interactions between light and matter is the collision of a photon with a free electron. When the energy of the incoming photon $\hbar\omega_0$ is much smaller than the mass energy $m_e c^2$ of the electron in the rest frame of the electron, the only process that has a significant probability of occurring is the scattering of the incident photon off of the electron; the scattering process at these energies is elastic and referred to as Thomson scattering. In this limit, the predictions from classical electrodynamics [1] are in complete agreement with the Klein-Nishina cross section [2] calculated with perturbative quantum electrodynamics (QED).

At moderate and higher energies, that is, when $\hbar\omega_0 \gtrsim m_e c^2$, the resulting inelastic-scattering process is referred to as Compton scattering or the Compton effect [3]. In this case, the process must be described with relativistic QED [4], and is second order in the fine-structure constant $\alpha \approx 1/137.036$. In addition, at these incident photon energies higher-order processes in α become significant. If the energy of the incoming photon is of the order of the electron mass energy but still below the threshold of electron-positron pair production, that is, $\hbar\omega_0 < 4m_e c^2$ (incident photon energy must be larger than $2m_e c^2$ because both momentum and energy must be conserved), the dominant higher-order process is double Compton scattering, or the double Compton effect, which is the focus of the present paper. By double Compton scattering we mean one photon collides with one electron and produces two photons in a single elementary event. This scattering process should not be confused with two single Compton scattering events, such as occurs when a photon scatters in succession from different electrons within a material [5]. Finally, there is also the nonlinear double Compton scattering process, where multiple photons are absorbed by an electron immersed in an intense laser field to generate two outgoing photons. This process, which must be treated by nonperturbative methods, has been a topic of recent theoretical study [6–9], but it is outside the scope of the present paper.

The first comprehensive treatment of the double Compton effect was given by Mandl and Skyrme [10] more than 50 years ago within the framework of perturbative QED. The classic treatise by Jauch and Rohrlich [11] further discusses and extends these results. Theoretical publications on this topic continue to appear (see, for example, the recent papers [12,13]). Experimental verification has also been ongoing, starting with the early pioneering measurements [14–16] and continuing with more recent [17–21] investigations.

In most studies of double Compton scattering, it is usually assumed that the initial photon and electron are in states of well-defined linear momentum; that is, they are described by plane waves. However, in recent decades, methods have been developed to generate beams of light with a helical phase front [22–25]. These *twisted* or *vortex* beams can carry an orbital angular momentum (OAM) in addition to the usual spin angular momentum [26–28]. The additional degree of freedom of OAM beams allows for novel applications. At visible wavelengths, many applications have been explored, such as in optical communications [29,30], the manipulation of microparticles [31,32], microscopy [33], and spectroscopy [34]. In recent years, numerous theoretical investigations have been conducted to study the effects of OAM beams in elementary interactions with atomic systems at optical and suboptical wavelengths, such as the modification of selection rules in atomic transitions [35,36], interaction with multielectron atoms and ions [37], novel effects in photoionization [38], and two-color above threshold ionization using XUV OAM beams combined with intense near-infrared laser radiation [39].

Usually beams of twisted photons in the visible range are generated by passing light through a fork hologram or spiral phase mask [40]. The same techniques have been attempted for the production of high-energy OAM beams in XUV and soft-x-ray ranges [41,42], but encountered difficulties associated with the damage threshold of the optical elements and low efficiencies at short wavelengths. These difficulties have motivated, during recent years, intense research on the generation of high-energy OAM beams, by means of high harmonic generation [43,44], which have recently been experimentally realized [45] for XUV beams, and through inverse Compton scattering [46–48]. The proposed setup in [48], for example, discusses the generation of photons carrying OAM in the soft-x-ray range.

At still higher energies, there are several proposals for the generation of OAM photon beams in the range of hard x rays and γ rays, based on the up-conversion of low-energy twisted photons through inverse Compton scattering from a beam of

*jsherwin99@hotmail.com

high-energy electrons [46,47], on nonlinear inverse Compton scattering [49], and through the interaction of an intense vortex laser with a plasma target [50]. The experimental realization of these setups would make accessible new phenomena in the relativistic QED regime involving OAM photon beams.

In addition, theoretical interest on the calculation of QED processes involving vortex beams is growing. A nonexhaustive selection of recent studies is [51–53]. To date, however, there have been no theoretical studies involving the double Compton scattering of twisted photons. Here, we take a step toward closing this gap in the literature.

In this paper, we investigate how the OAM of the incident gamma-ray photon affects the angular distribution of the pair of scattered photons resulting from the double Compton process and compare this to the results for plane-wave scattering. Specifically, calculations of the (triple) differential cross section, $d\sigma/dE_1 d\Omega_1 d\Omega_2$, have been performed for the scattering of high-energy photons prepared in Bessel states with different cone opening angles θ_p and orbital angular momentum m. Although the cross section does not depend on m, it is sensitive to the cone opening angle θ_p. The differential cross section was also found to be sensitive to the difference in orbital angular momentum Δm for incident photons prepared in a superposition of two Bessel states each having a different value of m.

The organization of the paper is as follows. In Sec. II, a preliminary discussion of the setup of the problem and a brief summary of the theory of the double Compton effect are given for plane waves. This is followed by the theoretical description of a photon prepared in a twisted Bessel state and the determination of the cross section for double Compton scattering of twisted photons. In Sec. III, the numerical results are discussed, first for a photon prepared in a Bessel state with well-determined orbital angular momentum projection m, and then for a superposition of twisted Bessel states. Finally, in Sec. IV, a summary of the main results and conclusions is given. Throughout the paper, we use rationalized MKS units and a space-time metric of $g^{\mu\nu} = \mathrm{diag}(1, -1, -1, -1)$.

II. THEORETICAL BACKGROUND

A. Setup of the problem

The basic setup to be analyzed is illustrated in Fig. 1(a). A beam of twisted photons each with total energy E_0 propagating along the z axis collides head on, i.e., at 180°, with a plane-wave electron with momentum $\vec{p}_i$. A photon from the beam interacts with the electron and engenders double Compton scattering. The scattered electron, also described as a plane wave with definite momentum $\vec{p}_f$, and two photons emerge from this single elementary process with momenta $\vec{p}_1$ and $\vec{p}_2$. That is, we project the scattered photon states onto basis states of definite momentum, which corresponds to what is usually measured by a detector in practice.

For each twisted photon of the incident beam, only the projection of the momentum onto the direction of the propagation of the beam, here taken to coincide with the positive z direction and designated $\vec{p}_{0z}$, is well defined, and has magnitude $|\vec{p}_{0z}| = \kappa_{p_\parallel}$. This also defines the direction of angular momentum projection. The transverse component of the incident twisted photon momentum has well-defined magnitude $|\vec{p}_{0\perp}| = \kappa_{p_\perp}$ but its direction is indeterminate. That is, the twisted photon state is a superposition of well-defined momentum states which sweep out a cone of opening angle θ_p and are specified through the azimuthal angle ϕ_p. The definitions of coordinates and angles that are used to characterize the incident and scattered photons are illustrated in Fig. 1(b).

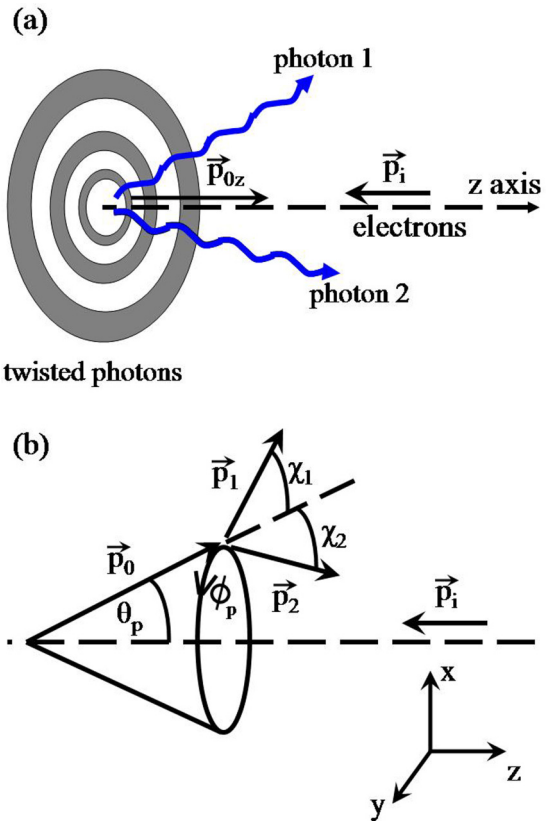

FIG. 1. Double Compton scattering of an incoming beam of high-energy twisted photons off of plane-wave electrons producing two photons (blue wavy arrows) in a single elementary process. (a) The twisted beam of photons collides head on with an oppositely propagating (under 180°) beam of plane-wave electrons moving with nonrelativistic speeds. (b) Definition of the coordinates and angles that are used to characterize the double Compton scattering process.

The details of describing the state of the twisted photons will be given later in the paper. Here we note that the transition amplitude for the twisted state is composed of the contributions from all the plane-wave components. In the discussion that follows, we shall briefly summarize the formalism for double Compton scattering when all particles are described by plane waves. In the following, the scalar product between two four-vectors is denoted by $a \cdot b = a^\mu b_\mu = a^0 b^0 - \vec{a} \cdot \vec{b}$, consistent with the choice of space-time metric, and contraction of the Dirac matrices γ^μ with a four-vector a is given by $\hat{a} = \gamma^\mu a_\mu$.

B. Differential cross section for plane-wave photons

A summary of the formalism to calculate the S matrix and differential cross section is given for the case of double Compton scattering of plane-wave photons. In the following, the incoming photon is not assumed to collide head on with the

electron but to be incident at $\theta_0 = \theta_p$, that is, the momentum cone opening angle of the twisted photon. This will serve as the starting point for developing the formalism for twisted photons in the following sections.

For reference in future discussions, the incoming and outgoing four-vectors of the electron are denoted by $p_{i,f} = (E_{i,f}/c, \vec{p}_{i,f})$, respectively, $\vec{n}_p = \vec{p}/|\vec{p}| = (\sin\theta\cos\varphi,\ \sin\theta\sin\varphi,\ \cos\theta)$ is the unit vector in the electron's propagation direction, and $u_\lambda(p)$ denotes the Dirac bispinor of definite helicity λ. The Dirac bispinors are normalized according to the convention $\bar{u}_\lambda u_\lambda = u_\lambda^\dagger \gamma^0 u_\lambda = 1$, and $\bar{u}_\lambda = u_\lambda^\dagger \gamma^0$ is the Dirac adjoint.

The momentum four-vectors of the photons are related to their propagation four-vectors by $p_j = \hbar k_j$, with $k_j = (\omega/c)\, n_j$, and where

$$n_j = (1, \vec{n}_j) = (1,\ \sin\theta_j\cos\phi_j,\ \sin\theta_j\sin\phi_j,\ \cos\theta_j) \quad (1)$$

is the unit four-vector, ϕ_j measures the azimuth, and θ_j measures the polar angle ($j = 0,1,2$). Here $j = 0$ denotes the incoming absorbed plane-wave photon, the values $j = 1,2$ correspond to the emitted photons, and $\vec{n}_j$ are the unit three-vectors denoting the propagation of the photons in space. Finally, the polarization four-vectors are denoted by ϵ^{α_j}, with ($j = 0,1,2$) denoting the photon according to the same correspondence as for the other four-vectors.

According to the Feynman rules of QED, the S matrix is given by [54]

$$S_{\rm PW} = i(2\pi\hbar)^4 \delta^{(4)}(p_i + p_0 - p_f - p_1 - p_2)\mathcal{M}, \quad (2)$$

where the δ function ensures the conservation of the four-momenta during scattering. The scattering amplitude $\mathcal{M}$ is given by

$$\mathcal{M} = \frac{m_e c^2 e^3}{\sqrt{8E_i E_f E_0 E_1 E_2 \epsilon_0^3 V^5}}\mathcal{N}, \quad (3)$$

with

$$\mathcal{N} = \sum_{i=1}^{6} N_i,$$

and where

$$\begin{aligned} N_1 &= \bar{u}_{\lambda'}(p_f)\hat{\epsilon}^{\alpha_2^*} G(p_f + p_2)\hat{\epsilon}^{\alpha_1^*} G(p_i + p_0)\hat{\epsilon}^{\alpha_0} u_\lambda(p_i), \\ N_2 &= \bar{u}_{\lambda'}(p_f)\hat{\epsilon}^{\alpha_2^*} G(p_f + p_2)\hat{\epsilon}^{\alpha_0} G(p_i - p_1)\hat{\epsilon}^{\alpha_1^*} u_\lambda(p_i), \\ N_3 &= \bar{u}_{\lambda'}(p_f)\hat{\epsilon}^{\alpha_0} G(p_f - p_0)\hat{\epsilon}^{\alpha_2^*} G(p_i - p_1)\hat{\epsilon}^{\alpha_1^*} u_\lambda(p_i), \end{aligned} \quad (4)$$

$N_4 = N_1\ (\alpha_1 \leftrightarrow \alpha_2)$, $N_5 = N_2\ (\alpha_1 \leftrightarrow \alpha_2)$, and $N_6 = N_3\ (\alpha_1 \leftrightarrow \alpha_2)$ in a self-explanatory notation, while G is the electron propagator.

The differential cross section is then obtained from the S matrix as [54]

$$d\sigma_{\rm PW} = \frac{1}{J_{\rm PW}}\frac{|S_{\rm PW}|^2}{T}\frac{V d^3p_f}{(2\pi\hbar)^3}\frac{V d^3p_1}{(2\pi\hbar)^3}\frac{V d^3p_2}{(2\pi\hbar)^3}, \quad (5)$$

where $J_{\rm PW} = c^3(p_i \cdot p_0)/(V E_0 E_i)$ is the incident flux for photons and electrons of well-defined momenta. Here, $d^3p_{1,2} = E_{1,2}^2 dE_{1,2} d\Omega_{1,2}/c^3$. The squared amplitude $|S_{\rm PW}|^2$ includes the Dirac δ of argument zero, $[\delta^{(4)}(p_i + p_0 - p_f - p_1 - p_2)]^2 = \delta^{(4)}(p_i + p_0 - p_f - p_1 - p_2) c T V (2\pi\hbar)^{-4}$, so that all factors of V and T in Eq. (5) cancel, as they should. Integration over the final electron momentum and the photon energy E_2 yields the final expression for the cross section, differential in E_1, Ω_1, and Ω_2, still dependent on the one incoming and two outgoing photon polarizations, and the electron spins, as [13]

$$\begin{aligned} \frac{d\sigma_{\rm PW}}{d\Gamma} &= \frac{d\sigma_{\rm PW}}{dE_1 d\Omega_1 d\Omega_2} \\ &= \frac{\alpha^3 m_e^2}{(2\pi\hbar)^2}\frac{E_1 E_2}{E_f\,(p_i \cdot p_0)}\left|\left(\frac{\partial(E_f + E_2)}{\partial E_2}\right)^{-1}\right| \\ &\quad \times |\mathcal{N}|^2 \Theta(E_2)\Theta(E_f - m_e c^2), \end{aligned} \quad (6)$$

where $d\Gamma = dE_1 d\Omega_1 d\Omega_2$ is the phase-space volume element of the scattered photons. In Eq. (6), the final four-momentum of the electron is $p_f = p_i + p_0 - p_1 - p_2$,

$$E_2 = c\left(\frac{p_i \cdot (p_1 - p_0) + p_0 \cdot p_1}{n_2 \cdot (p_1 - p_0 - p_i)}\right), \quad (7)$$

and the Dirac δ function associated with the integration of Eq. (5) over E_2 generates a Jacobian factor:

$$\frac{d(E_f + E_2)}{dE_2} = 1 + \left(\frac{E_2 + c[\vec{n}_2 \cdot (\vec{p}_1 - \vec{p}_0 - \vec{p}_i)]}{E_f}\right). \quad (8)$$

The step functions $\Theta(\cdot)$ at the end of Eq. (6) are needed since there are values of the angles for which $E_2 > 0$, from Eq. (7), but $E_f < m_e c^2$. If, as in the present paper, the initial electron and incoming photon are unpolarized, and the polarization of all final particles is unobserved, then $|\mathcal{N}|^2$ in Eq. (6) is replaced by the sum-averaged quantity

$$\overline{|\mathcal{N}|^2} = \frac{1}{4}\sum_{\lambda\lambda'}\sum_{\alpha_0\alpha_1\alpha_2}|\mathcal{N}|^2. \quad (9)$$

Although in this paper $\overline{|\mathcal{N}|^2}$ is calculated numerically, an analytical expression for this quantity exists for the case of double Compton scattering of plane-wave photons off of electrons at rest and can be found, for example, in [10] or in the textbook by Jauch and Rohrlich [11], Eq. (11)–(35).

Finally, the cross section of Eq. (6) diverges whenever ω_1 or ω_2 goes to zero. This is the so-called infrared catastrophe of QED. The breakdown of Eq. (6) indicates that radiative corrections must be included into the calculation of the cross section. However, as thoroughly discussed in [13], for the energy of the photons considered in this paper, i.e., $\hbar\omega_0 \sim 1$ MeV, the infrared radiative corrections should not exceed a few percent.

In an experiment, the detectors can only detect photons above a certain threshold energy. In the experiment of [16], for example, only photons with an energy above 13 keV were detected. This threshold is included theoretically by employing a cutoff energy ϵ_c. That is, when integrating over the energy of a scattered photon, only photon energies above the fixed energy cutoff ϵ_c are included. Likewise, the values of parameters used in calculation are chosen such that neither scattered photon energy falls below the fixed cutoff energy.

C. Twisted photon states and the twisted cross section

A mathematically convenient representation of a photon in a twisted Bessel state with definite helicity Λ and *total* angular momentum (TAM) projection m is given by [46,52,55]

$$|\kappa_{p_\perp}\kappa_{p_\parallel} m\Lambda\rangle = \int \frac{V d^3p_0}{(2\pi\hbar)^3} b_{\kappa_{p_\perp}\kappa_{p_\parallel} m}(\vec{p}_0)|\vec{p}_0\Lambda\rangle, \tag{10}$$

where

$$b_{\kappa_{p_\perp}\kappa_{p_\parallel} m}(\vec{p}_0) = N_{\rm tw}\delta(p_{0_z} - \kappa_{p_\parallel}) a_{\kappa_{p_\perp} m}(\vec{p}_{0_\perp}), \tag{11}$$

and the transverse amplitude $a_{\kappa_{p_\perp} m}(\vec{p}_{0_\perp})$ is defined as

$$a_{\kappa_{p_\perp} m}(\vec{p}_{0_\perp}) = \sqrt{\frac{2\pi\hbar}{\kappa_{p_\perp}}}(-i)^m e^{im\phi_p}\delta(|\vec{p}_{0_\perp}| - \kappa_{p_\perp}). \tag{12}$$

The normalization factor $N_{\rm tw}$ that appears in the definition of the amplitude $b_{\kappa_{p_\perp}\kappa_{p_\parallel} m}(\vec{p}_0)$ is determined such that the twisted Bessel states satisfy the normalization [52]

$$\begin{aligned}&\langle\kappa_{p_\perp}\kappa_{p_\parallel} m\Lambda|\kappa'_{p_\perp}\kappa'_{p_\parallel} m'\Lambda'\rangle \\ &\quad= \frac{2\pi^2\hbar^2}{RL_z}\delta_{mm'}\delta_{\Lambda\Lambda'}\delta(\kappa_{p_\perp} - \kappa'_{p_\perp})\delta(\kappa_{p_\parallel} - \kappa'_{p_\parallel}).\end{aligned} \tag{13}$$

This corresponds to a normalization of one particle per cylindrical volume $V = \pi R^2 L_z$, where both radius R and length L_z are made to go to infinity (for details, see especially [52]).

To calculate the differential cross section, we have to square the twisted S matrix given by [46,55]

$$S_{\rm tw} = \int \frac{V d^3p_0}{(2\pi\hbar)^3} b_{\kappa_{p_\perp}\kappa_{p_\parallel} m}(\vec{p}_0) S_{\rm PW}(\vec{p}_0). \tag{14}$$

From $|S_{\rm tw}|^2$, the cross section, differential in E_1, Ω_1, and Ω_2, for twisted photons incident on plane-wave electrons in a head-on collision is given by [47,55]

$$\frac{d\sigma_{\rm tw}}{d\Gamma} = \frac{d\sigma_{\rm tw}}{dE_1 d\Omega_1 d\Omega_2} = \int \frac{d\phi_p}{2\pi}\frac{d\sigma_{\rm PW}(\theta_p,\phi_p)}{dE_1 d\Omega_1 d\Omega_2}, \tag{15}$$

where $d\Gamma = dE_1 d\Omega_1 d\Omega_2$. Unlike $S_{\rm tw}$ in Eq. (14), which depends on θ_p and m, both $|S_{\rm tw}|^2$ and $d\sigma_{\rm tw}$ are independent of m [55], but still depend on the cone opening angle θ_p.

Finally, so far the twisted photon has been considered to have well-defined helicity Λ and well-defined TAM projection m. In this paper, we assume that the photon is twisted but *unpolarized*. In this case, the spin angular momentum averages to zero, but the photon still carries definite OAM through its helical phase-front structure [35]. Therefore, we shall consider m the OAM projection of the incoming twisted, but unpolarized, photon.

III. DISCUSSION OF RESULTS

For numerical calculations, we consider the specific case of a γ-ray photon, prepared in a twisted Bessel state, colliding with an electron initially at rest. That is, we perform the calculation in the rest frame of the initial electron. This choice is a good approximation for scattering of γ rays from electrons in target materials the work functions of which are negligible relative to the energy of the photon and can be considered quasifree. The calculation is also suitable for free electrons as emitted from an electron gun, provided that their kinetic energy is much smaller than the rest mass energy of the electron. For electron beams, where the electrons are moving in the laboratory frame, the observed results can be obtained by performing a Lorentz transformation on the results in the rest frame. For electron beams with low kinetic energy, $E_{\rm kin} \lesssim 1$ keV, the results of calculations performed in the rest frame and the laboratory frame will differ very little. Finally, we choose photons such that the recoil parameter is at least

$$r_0 = \frac{\hbar\omega_0}{m_e c^2} \sim 1, \tag{16}$$

as it is well known that, unlike the cross section for the single Compton effect, which remains finite with recoil parameter $r_0 \ll 1$, the cross section for the double Compton effect becomes completely negligible.

A. Energy range of scattered photons

For the usual case of double Compton scattering of a plane-wave photon on a plane-wave electron, the energy of the second photon is completely determined by Eq. (7), once the scattering angles of both photons and the energy of the first photon are specified.

For double Compton scattering of a twisted photon of definite opening angle θ_p, the energy of the second scattered photon is not definitely determined from the scattering angles of the scattered photons and energy of the first photon, but depends on ϕ_p through the effective scattering angles $\chi_1(\phi_p)$ and $\chi_2(\phi_p)$. Specifically, for an incident twisted photon traveling in the positive z direction and electron initially at rest, pertinent to the calculations considered here, Eq. (7) yields

$$E_2(\phi_p) = \frac{E_0 - E_1 - \frac{E_0 E_1}{m_e c^2}[1 - \cos\chi_1(\phi_p)]}{1 + \frac{E_0}{m_e c^2}[1 - \cos\chi_2(\phi_p)] - \frac{E_1}{m_e c^2}(1 - \cos\chi_{12})}, \tag{17}$$

with

$$\begin{aligned}\cos\chi_1(\phi_p) &= \vec{n}_1\cdot\vec{n}_0(\phi_p) \\ &= \sin\theta_p\sin\theta_1\cos(\phi_p - \phi_1) + \cos\theta_p\cos\theta_1,\end{aligned} \tag{18}$$

$$\begin{aligned}\cos\chi_2(\phi_p) &= \vec{n}_2\cdot\vec{n}_0(\phi_p) \\ &= \sin\theta_p\sin\theta_2\cos(\phi_p - \phi_2) + \cos\theta_p\cos\theta_2,\end{aligned} \tag{19}$$

and

$$\begin{aligned}\cos\chi_{12} &= \vec{n}_1\cdot\vec{n}_2 \\ &= \sin\theta_1\sin\theta_2\cos(\phi_1 - \phi_2) + \cos\theta_1\cos\theta_2,\end{aligned} \tag{20}$$

associated with the plane-wave component of the twisted photon parametrized by ϕ_p.

As the parameter ϕ_p varies over the interval $[0,2\pi]$, the plane-wave component sweeps out a cone in momentum space, changing the effective scattering angles $\chi_1(\phi_p)$ and

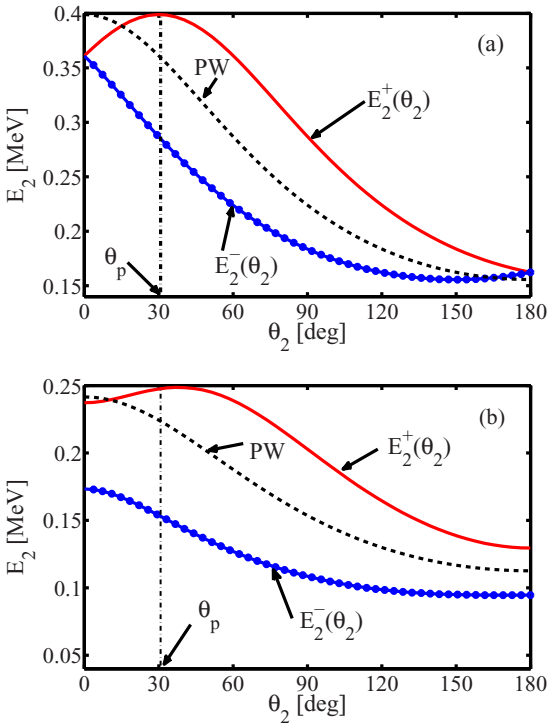

FIG. 2. Energy range of the second scattered photon for double Compton scattering of the twisted incident photon, of energy $E_0 = 0.4$ MeV and momentum cone opening angle $\theta_p = 30^\circ$, on an electron initially at rest. The other photon (first scattered photon) scatters with well-defined energy and scattering angle. (a) The allowed energies of the second scattered photon (region between red solid line and blue line with filled circles) as a function of θ_2 and with $\phi_2 = 90^\circ$; the first photon scatters at angle $\theta_1 = 35^\circ$, and $\phi_1 = 0^\circ$, with energy $E_1 = 1$ keV. (b) The allowed energies of the second scattered photon as a function of θ_2. All parameters are the same as in Fig. 2(a), except $E_1 = 150$ keV.

$\chi_2(\phi_p)$ of the scattered photons relative to the direction of that plane-wave component. The energy E_2 of the second scattered photon will be unique for each plane-wave component of the twisted photon, but will involve a spectrum of energies for the twisted photon as a whole.

The range of allowed energies for the second scattered photon $E_2^-(\theta_2) \leqslant E_2 \leqslant E_2^+(\theta_2)$ is indicated by the region between the solid red line $[E_2^+(\theta_2)]$ and the blue line with filed circles $[E_2^-(\theta_2)]$ in Figs. 2(a) and 2(b) for $E_1 = 1$ and 150 keV, respectively. The energy of the incident twisted photon is $E_0 = 0.4$ MeV, with opening angle $\theta_p = 30^\circ$, and the first scattered photon scatters at angles $\theta_1 = 35^\circ$ and $\phi_1 = 0^\circ$. The spectral envelope functions, $E_2^+(\theta_2)$ and $E_2^-(\theta_2)$, characterizing the extreme bounds of the energy spectrum of the second scattered photon, are obtained by finding the maximum and minimum of $E_2(\phi_p)$ in Eq. (17) with respect to ϕ_p while keeping all other independent variables fixed. After a straightforward but lengthy calculation, they are given by

$$E_2^\pm(\theta_2) = \frac{E_0 - E_1 - \frac{E_0 E_1}{m_e c^2}(1 - \eta_1^\pm)}{1 + \frac{E_0}{m_e c^2}(1 - \eta_2^\pm) - \frac{E_1}{m_e c^2}(1 - \cos\chi_{12})}, \tag{21}$$

where

$$\eta_1^\pm = X_\pm \sin\theta_p \sin\theta_1 + \cos\theta_p \cos\theta_1, \tag{22}$$

$$\eta_2^\pm = \sin\theta_p \sin\theta_2 (X_\pm \cos\phi + Y_\pm \sin\phi) + \cos\theta_p \cos\theta_2, \tag{23}$$

$$X_\pm = \pm\sqrt{1 - Y_\pm^2}, \tag{24}$$

and

$$Y_\pm = \frac{F_2 F_3 \pm F_1\sqrt{F_1^2 + F_2^2 - F_3^2}}{F_1^2 + F_2^2}, \tag{25}$$

where $\phi = \phi_2 - \phi_1$, and without loss of generality we set $\phi_1 = 0$. The quantities F_1, F_2, and F_3, which are functions of θ_p, θ_1, θ_2, ϕ, $r_0 = E_0/m_e c^2$, $r_1 = E_1/m_e c^2$, and $\Delta E = E_0 - E_1$, are given by

$$\begin{aligned} F_1 &= r_0 \sin\theta_p \sin\theta_1 \sin\phi[\Delta E - r_0 E_1(1 - \cos\theta_p \cos\theta_1)], \\ F_2 &= \big[r_0 E_1 - E_0 r_1^2(1 - \cos\chi_{12}) \\ &\quad + E_1 r_0^2(1 - \cos\theta_p \cos\theta_2)\big] \sin\theta_p \sin\theta_1 \\ &\quad + \big[r_0 \Delta E - r_0^2 E_1(1 - \cos\theta_p \cos\theta_1)\big] \sin\theta_p \sin\theta_2 \cos\phi, \\ F_3 &= r_0^2 E_1 \sin^2\theta_p \sin\theta_1 \sin\theta_2 \sin\phi. \end{aligned} \tag{26}$$

In Fig. 2(a), the energy of the first scattered photon is $E_1 = 1$ keV, which is essentially negligible in comparison to the energy of the incident photon. In this case, Eq. (17) reduces to $E_2(\phi_p) \approx E_0/\{1 + \frac{E_0}{m_e c^2}[1 - \cos\chi_2(\phi_p)]\}$, and the spectral envelope functions of Eq. (21) become $E_2^\pm(\theta_2) \approx E_0/[1 + \frac{E_0}{m_e c^2}(1 - \eta_2^\pm)]$, where $\eta_2^\pm \approx \cos(\theta_p \mp \theta_2)$. The results are, therefore, nearly identical to those for single Compton scattering of a twisted photon, and have a simple interpretation. The upper bound $E_2^+(\theta_2)$ of the energy spectrum arises from the plane-wave component that is maximally aligned with the second scattered photon momentum $\vec{p}_2$. For this case, $\phi_p = \phi_2$ and the smallest effective scattering angle $\chi_2(\phi_p) = |\theta_p - \theta_2|$. The lower bound $E_2^-(\theta_2)$ corresponds to the largest effective scattering angle $\chi_2(\phi_p) = \theta_p + \theta_2$, which occurs (in radian) at $\phi_p = \phi_2 + \pi$. The dependence of the second photon energy on scattering angle with all conditions identical except for the incident plane-wave photon is plotted as the black dashed curve (PW) in the figure for comparison. The maximum energy $E_2 \approx E_0$ is essentially the same for plane-wave and twisted photons when the first photon is very soft, but the maximum shifts from $\theta_2 = 0$, for plane-wave photons, to $\theta_2 \approx \theta_p$ for twisted photons.

In Fig. 2(b), the energy of the first scattered photon is $E_1 = 150$ keV, which is a significant fraction of the energy of the incident photon. In this case, no simplifications to Eqs. (17) and (21) are possible. However, several interesting results are observed. First, when $\theta_2 = 0$ or 180°, the spectral envelopes no longer converge to a common value, like the case when $E_1 \to 0$. In the limit where $E_1 \to 0$, the energy $E_2(\phi_p)$ becomes independent of ϕ_p when $\theta_2 = 0$ or 180°. However, when E_1 is not zero, the symmetry of $E_2(\phi_p)$ with respect to ϕ_p is broken, even for axial scattering of the second photon, and a gap in

the spectral envelope results, which increases with increasing E_1. Secondly, the angle θ_2 at which the energy of the second scattered photon reaches a maximum no longer coincides with the momentum cone opening angle θ_p of the incident twisted beam.

B. Differential cross section for the scattering of a twisted photon with well-defined OAM

The twisted triple differential cross section of Eq. (15) is evaluated numerically for selected values of the input parameters E_0, θ_p, E_1, and θ_1, while the angles θ_2 and ϕ_2 are varied over all values compatible with kinematic constraints. The angle $\phi_1 = 0^\circ$, which fixes the orientation of the coordinate system. The energy E_2 is not independent, but is determined by the other input parameters according to Eq. (17). The cross section is averaged over the helicity of the incoming twisted photon and the initial electron, as they are both assumed to be unpolarized with respect to spin degree of freedom, and the final helicities of the scattered photons and scattered electron are summed over, as they are not observed. The evaluation of the matrix element of Eq. (3) is performed by explicit matrix multiplication using the standard Dirac representation of the Clifford algebra. This numerical implementation was tested for correctness in two ways. First, it was tested for gauge invariance. That is, the cross section is invariant under the gauge transformation $\epsilon_j \to \epsilon_j + Ck_j$, for each $j = 1,2$ separately, and C is an arbitrary constant. Second, the case where $\theta_p = 0^\circ$ should reproduce the results for the double Compton effect with incident plane-wave photons. The results of the code for $\theta_p = 0^\circ$ were therefore checked against a separately written code that implements the analytical formula for the triple differential cross section given in [10], and they were found to be in complete agreement. Finally, the triple differential cross section calculated, as just described, as a function of the angles θ_2 and ϕ_2 shall be referred to as the angular distribution of the second scattered photon or, more briefly, as the angular distribution.

The results for the twisted triple differential cross section, defined in Eq. (15), for the incident twisted photon of energy $E_0 = 0.4$ MeV, on an electron at rest, are shown in Fig. 3 as a function of the angles θ_2 and ϕ_2 of the second scattered photon, for several choices of momentum cone opening angle θ_p. The energy of the first scattered photon is $E_1 = 50$ keV, its polar angle $\theta_1 = 35^\circ$, and its azimuthal angle is fixed here and in all further results to $\phi_1 = 0^\circ$. This corresponds to a choice for the coordinate system such that ϕ_2 is the azimuthal angle of the second scattered photon relative to the first. This also implies that the x-z plane, which contains the average propagation direction of the incident twisted photon and the first scattered photon, is a symmetry plane, and the angular distributions of the differential cross section reflect this symmetry.

The well-known results for incoming plane-wave photons ($\theta_p = 0^\circ$) are shown in Fig. 3(a). These results indicate that the second photon tends to scatter at large polar angles ($\theta_2 > 90^\circ$) relative to the small polar angle ($\theta_1 = 35^\circ$) of the first scattered photon, and also tends to scatter preferentially into the $x \geqslant 0$ half space, that is, the same half space containing the first photon, for most polar angles.

For increasing values of the cone opening angle $\theta_p > 0^\circ$, the angular distribution gradually changes, and its peak magnitude decreases. Specific results for opening angles $\theta_p = 30$ and 60° and the theoretical limiting (and inaccessible to experiment) opening angle $\theta_p = 90^\circ$ are shown in Figs. 3(b), 3(c), and 3(d), respectively. Most notably, the angular distribution shifts such that the second photon now tends to scatter into the $x < 0$ half space and, as θ_p becomes sufficiently large, develops a distinct peak distributed around $\phi_2 = 180^\circ$.

Calculated angular distributions are shown in Fig. 4, for the first photon scattered into $\theta_1 = 145^\circ$. All other parameters are identical to those chosen for Fig. 3. The results for initial plane-wave photons ($\theta_p = 0^\circ$) are shown in Fig. 4(a). In this case, the second photon tends to scatter into the forward direction ($\theta_2 < 90^\circ$), concentrated in the $x < 0$ half space at azimuthal angles distributed around the peak located at $\phi_2 = 180^\circ$.

The angular distributions for cone opening angles $\theta_p = 30$, 60, and 90° are shown in Figs. 4(b), 4(c), and 4(d), respectively. In this case, an increase in cone opening angle, $\theta_p > 0^\circ$, tends to enhance the already predominately forward scattering ($\theta_2 < 90^\circ$) of the second photon, but it does so over the entire range of $0 \leqslant \phi_2 < 360^\circ$. Overall the angular distribution becomes more uniform with respect to ϕ_2.

To examine the effects of greater twisted photon energy, the angular distributions for an incident twisted photon of $E_0 = 2$ MeV, scattering on an electron at rest, are shown in Fig. 5. The energy of the first scattered photon is $E_1 = 150$ keV, with scattering angles $\theta_1 = 35^\circ$ and $\phi_1 = 0^\circ$. The well-known results for plane-wave photons ($\theta_p = 0^\circ$) are shown in Fig. 5(a). As expected, the second photon tends to scatter into a forward direction ($\theta_2 < 90^\circ$) and into the $x < 0$ half space with peak scattering centered around $\phi_2 = 180^\circ$.

As the cone opening angle $\theta_p > 0^\circ$ increases, the angular distribution undergoes pronounced changes. These changes are documented in the results for opening angles $\theta_p = 30$, 60, and 90°, as shown in Figs. 5(b), 5(c), and 5(d), respectively. In contrast to the results presented in Fig. 4 for $E_0 = 0.4$ MeV, increasing $\theta_p > 0^\circ$ increasingly shifts the angular distribution away from scattering in the forward direction ($\theta_2 < 90^\circ$) and likewise shifts the angular distribution away from scattering predominately in the $x < 0$ half space centered about $\phi_2 = 180^\circ$, and into the $x > 0$ half space.

Corresponding results for $\theta_1 = 145^\circ$ are shown in Fig. 6. All other parameters are identical to those in Fig. 5. The results for an incident plane-wave photon are shown in Fig. 6(a). Like the case for which $\theta_1 = 35^\circ$, the angular distribution is strongly concentrated in the forward scattering direction and shows a strong tendency for the second photon to scatter into the $x < 0$ half space with peak scattering centered around $\phi_2 = 180^\circ$.

The results for opening angles $\theta_p = 30$, 60, and 90°, are shown in Figs. 6(b), 6(c), and 6(d), respectively. Like the results presented in Fig. 5, the angular distribution shifts toward larger θ_2 with increasing cone opening angle θ_p and ϕ_2 shifts from predominately in the $x < 0$ half space to ϕ_2 predominately in the $x > 0$ half space.

The previous, somewhat qualitative, discussion indicates that the angular distributions are sensitive to the cone opening angle θ_p and the energy E_0 of the incident twisted photon. In order to formulate a quantitative measure of this dependence,

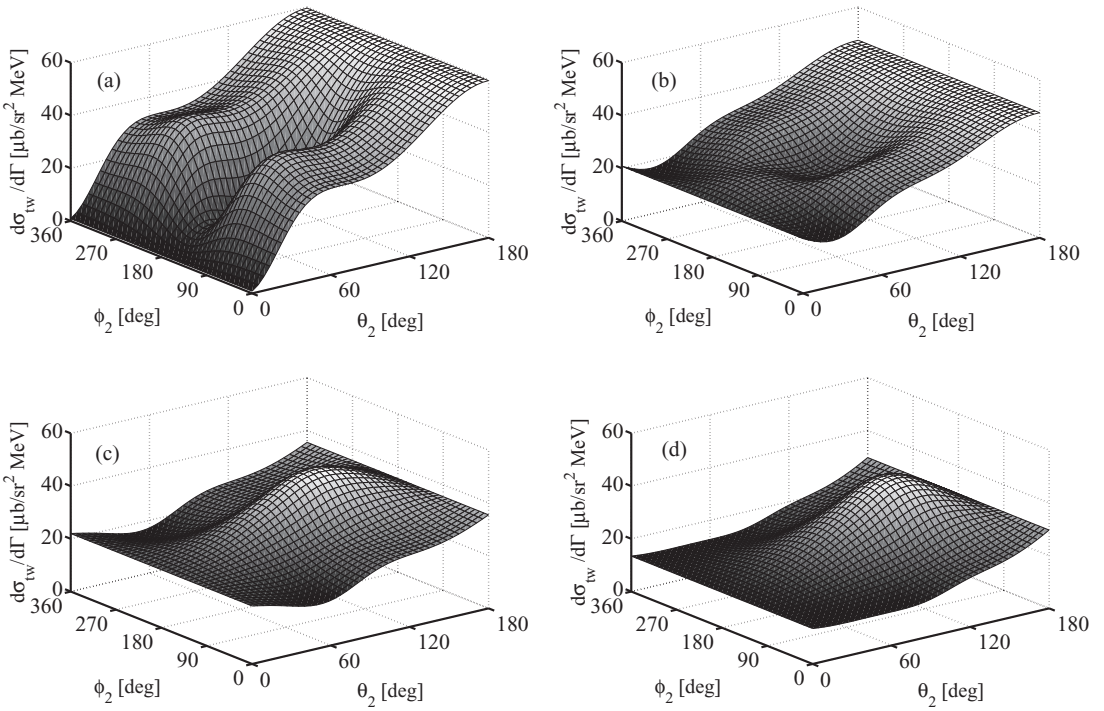

FIG. 3. Differential cross section $d\sigma_{\rm tw}/d\Gamma$, with $d\Gamma = dE_1 d\Omega_1 d\Omega_2$, plotted as a function of the scattering angles θ_2 and ϕ_2, for several choices of momentum cone opening angle θ_p of the incident twisted photon, with energy $E_0 = 0.4$ MeV, scattering on an electron at rest. Momentum cone opening angle (a) $\theta_p = 0^\circ$, which is identical to the results when incident plane-wave photons are used, (b) $\theta_p = 30^\circ$, (c) $\theta_p = 60^\circ$, and (d) $\theta_p = 90^\circ$, which is a theoretically limiting case that cannot be reached by experiment. The parameters for the other scattered photon (first scattered photon) are $\theta_1 = 35^\circ$, with $\phi_1 = 0^\circ$, and $E_1 = 50$ keV.

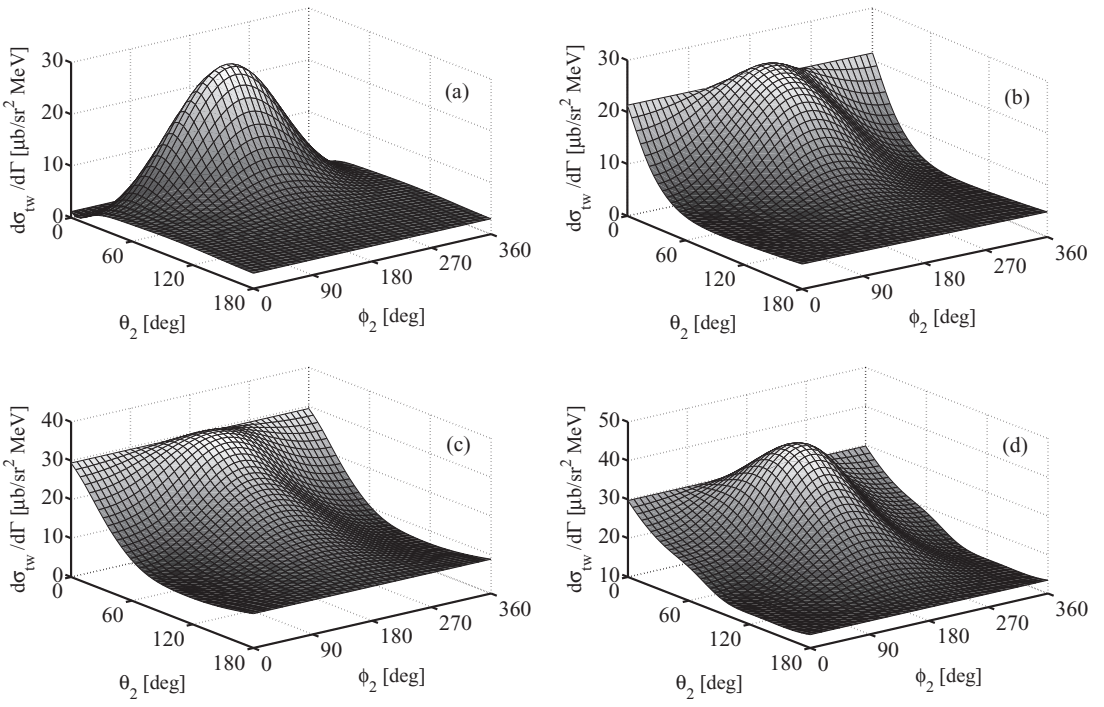

FIG. 4. Differential cross section $d\sigma_{\rm tw}/d\Gamma$, with $d\Gamma = dE_1 d\Omega_1 d\Omega_2$, plotted as a function of the scattering angles θ_2 and ϕ_2, for several choices of momentum cone opening angle θ_p of the incident twisted photon, and the electron is initially at rest. Opening angle (a) $\theta_p = 0^\circ$, identical to the use of incident plane-wave photons, (b) $\theta_p = 30^\circ$, (c) $\theta_p = 60^\circ$, and (d) $\theta_p = 90^\circ$, a theoretically limiting value inaccessible to experiment. All other parameters are the same as for the calculations of Fig. 3, except $\theta_1 = 145^\circ$.

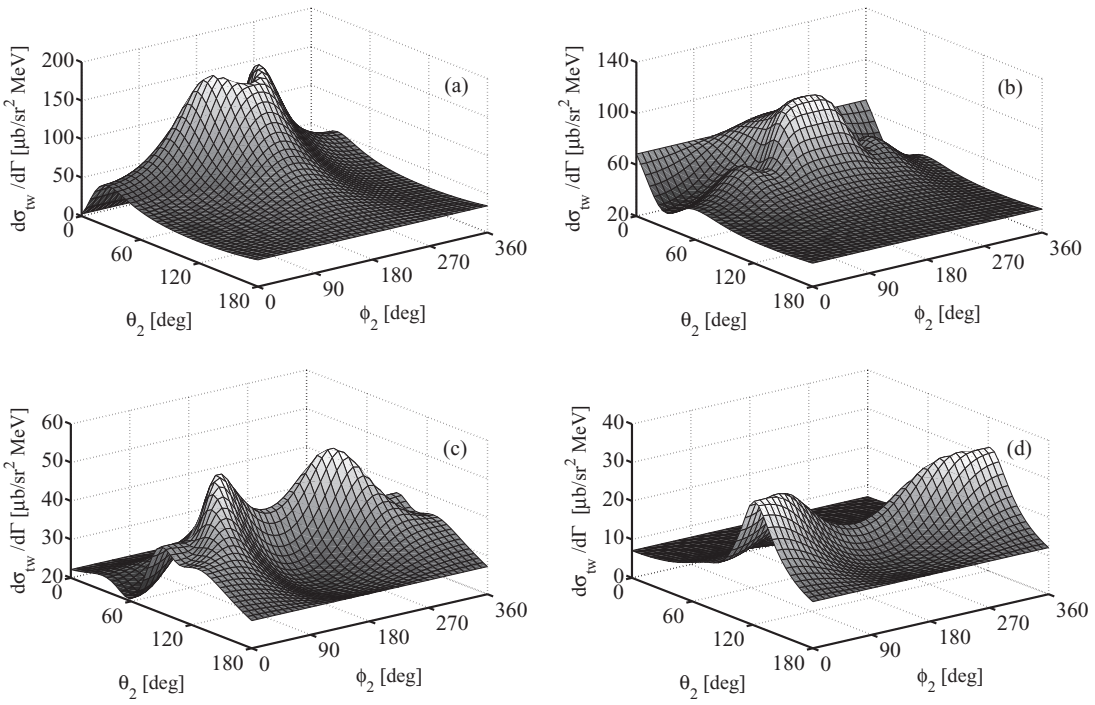

FIG. 5. Differential cross section $d\sigma_{\rm tw}/d\Gamma$, with $d\Gamma = dE_1 d\Omega_1 d\Omega_2$, plotted as a function of the scattering angles θ_2 and ϕ_2 for several choices of momentum cone opening angle θ_p of the incident twisted photon with energy $E_0 = 2.0$ MeV scattering on an electron at rest. Momentum cone opening angle (a) $\theta_p = 0^\circ$, (b) $\theta_p = 30^\circ$, (c) $\theta_p = 60^\circ$, and (d) $\theta_p = 90^\circ$. The parameters for the first scattered photon are $\theta_1 = 35^\circ$, and $\phi_1 = 0^\circ$, with $E_1 = 150$ keV.

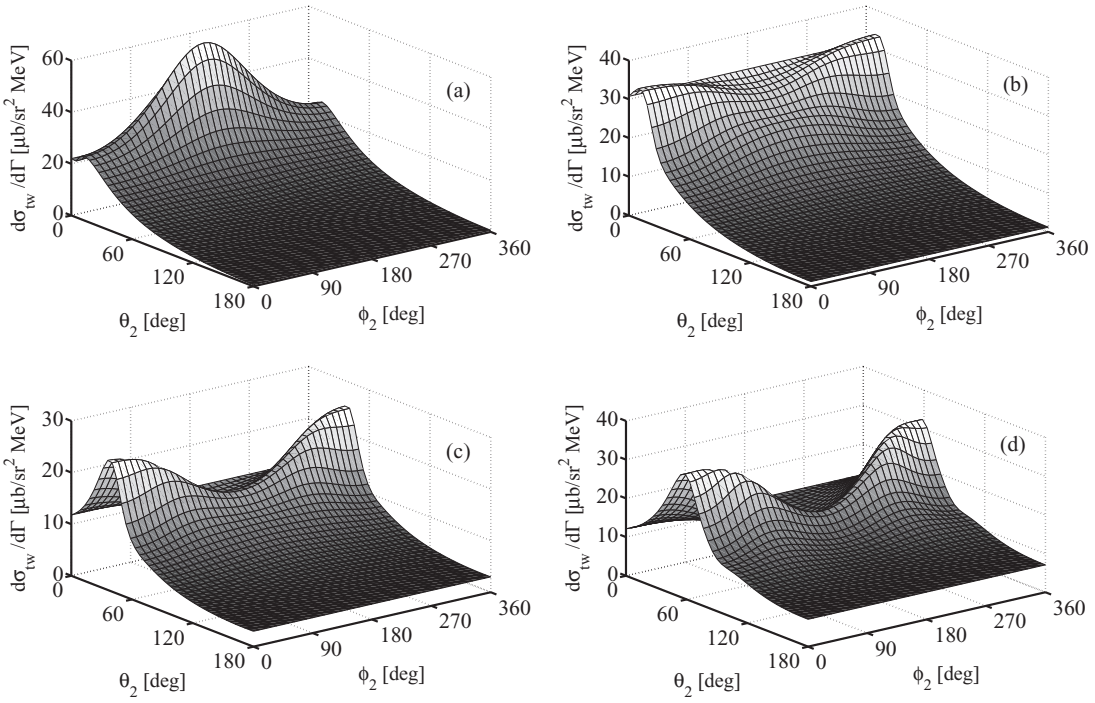

FIG. 6. Differential cross section $d\sigma_{\rm tw}/d\Gamma$, with $d\Gamma = dE_1 d\Omega_1 d\Omega_2$, plotted as a function of the scattering angles θ_2 and ϕ_2 for several choices of momentum cone opening angle θ_p of the incident twisted photon with energy $E_0 = 2.0$ MeV scattering on an electron at rest. (a) $\theta_p = 0^\circ$, (b) $\theta_p = 30^\circ$, (c) $\theta_p = 60^\circ$, and (d) $\theta_p = 90^\circ$. All other parameters are the same as for the calculations of Fig. 5, except $\theta_1 = 145^\circ$.

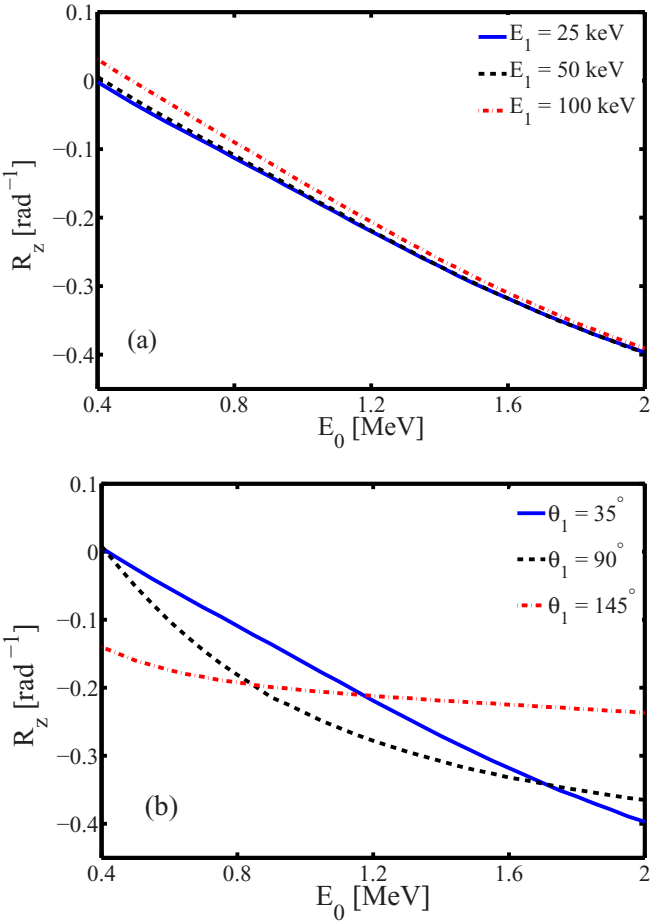

FIG. 7. Average rate of change $R_z = \Delta A_z/\Delta\theta_p$ of forward ($z > 0$ half-space) to backward ($z < 0$ half-space) scattering asymmetry with respect to momentum cone opening angle θ_p plotted as a function of incident twisted photon energy E_0. (a) $R_z(E_0)$ is plotted for several values of E_1, and $\theta_1 = 35°$, and (b) $R_z(E_0)$ is plotted for several values of θ_1, and $E_1 = 50$ keV.

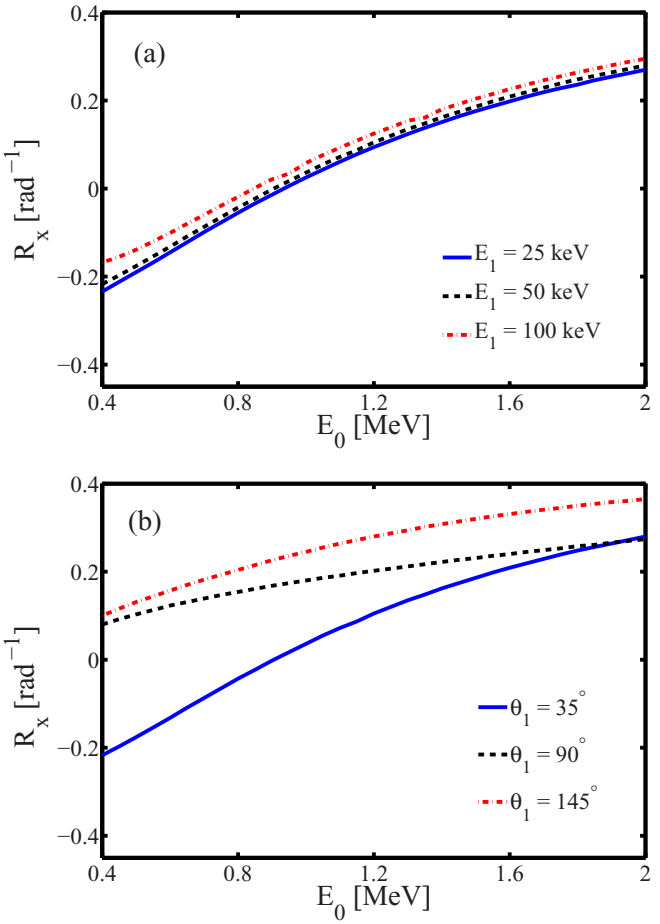

FIG. 8. Average rate of change $R_x = \Delta A_x/\Delta\theta_p$ of the $x > 0$ half-space to $x < 0$ half-space scattering asymmetry with respect to momentum cone opening angle θ_p plotted as a function of incident twisted photon energy E_0. (a) $R_x(E_0)$ is plotted for several values of E_1, and $\theta_1 = 35°$, and (b) $R_x(E_0)$ is plotted for several values of θ_1 and $E_1 = 50$ keV.

we define the following asymmetry parameters:

$$A_{x,(z)}(\theta_p) = \frac{\Sigma_{+x,(+z)}(\theta_p) - \Sigma_{-x,(-z)}(\theta_p)}{\Sigma_{+x,(+z)}(\theta_p) + \Sigma_{-x,(-z)}(\theta_p)}, \tag{27}$$

where

$$\Sigma_{+x,(+z)}(\theta_p) = \int_{x>0,(z>0)} d\Omega_2 \frac{d\sigma_{\rm tw}}{dE_1 d\Omega_1 d\Omega_2} \tag{28}$$

and

$$\Sigma_{-x,(-z)}(\theta_p) = \int_{x<0,(z<0)} d\Omega_2 \frac{d\sigma_{\rm tw}}{dE_1 d\Omega_1 d\Omega_2}. \tag{29}$$

In these definitions, the subscripts before the commas correspond to the asymmetry parameter A_x, and the subscripts in parentheses after the commas correspond to the asymmetry parameter A_z. For example, for an angular distribution with scattering entirely into half space $z > 0$, $\Sigma_{+z} = 1$ and $\Sigma_{-z} = 0$, yielding $A_z = 1$. For scattering entirely into half space $z < 0$, $\Sigma_{+z} = 0$ and $\Sigma_{-z} = 1$, hence $A_z = -1$. Finally, for any angular distribution with reflection symmetry with respect to the x-y plane, $\Sigma_{+z} = 0.5$ and $\Sigma_{-z} = 0.5$, and therefore $A_z = 0$.

The asymmetry parameters A_x and A_z can be used to quantify the sensitivity of the shift of the angular distribution to changes in cone opening angle θ_p. We define an overall average rate or change in the asymmetry A_x (A_z) per radian increase of θ_p as

$$R_{x,(z)} = \frac{\Delta A_{x,(z)}}{\Delta\theta_p} = \frac{A_{x,(z)}(\theta_{p_2}) - A_{x,(z)}(\theta_{p_1})}{\theta_{p_2} - \theta_{p_1}}. \tag{30}$$

As the investigations in this paper are not restricted to paraxial beams ($\theta_p \ll 1$ rad), but explore the full theoretical range of cone opening angles, we take $\theta_{p_1} = 0$ rad and $\theta_{p_2} = \pi/2$ rad.

Numerical results for R_z versus the energy of incident twisted photon E_0 are displayed in Fig. 7. The results are shown for selected values of the energy E_1 for $\theta_1 = 35°$ in Fig. 7(a), whereas, in Fig. 7(b), results are displayed for selected values of θ_1, while $E_1 = 50$ keV. The parameter R_z becomes increasingly more negative as E_0 increases. Hence, increases in the cone opening angle θ_p become ever more effective at shifting the angular distribution toward larger

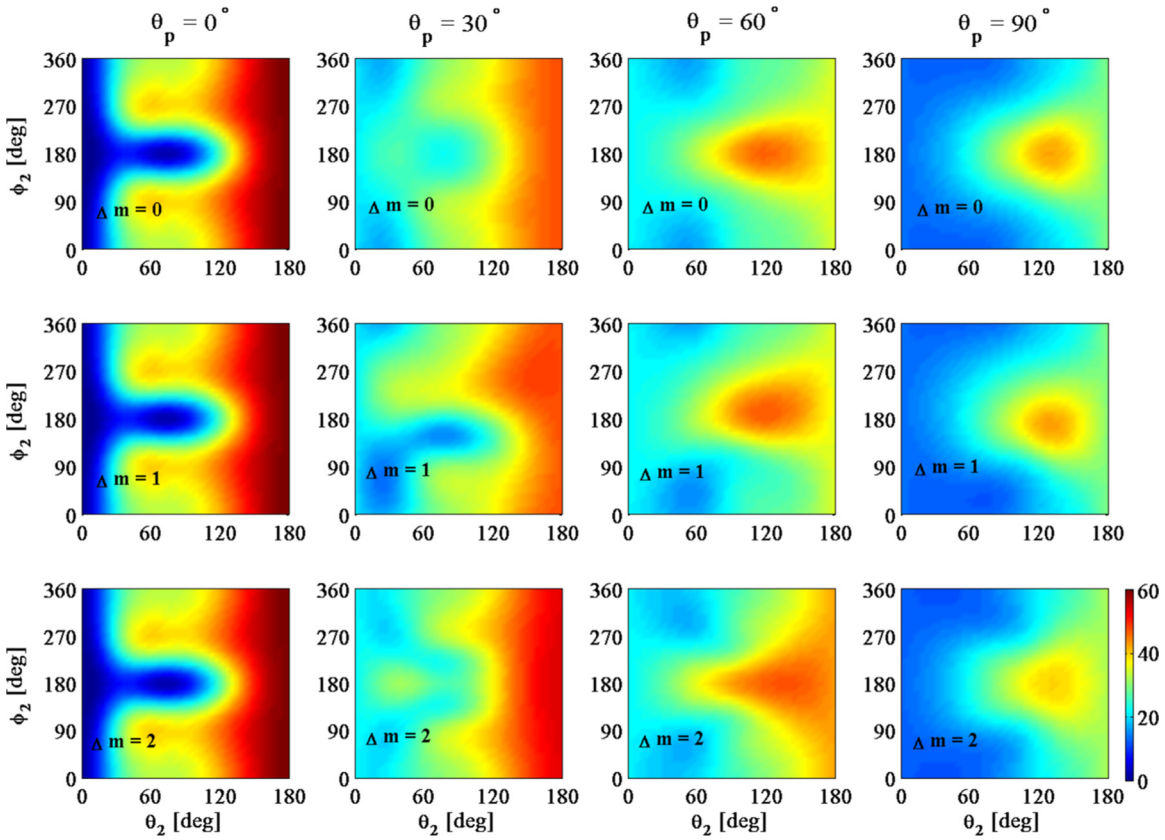

FIG. 9. Differential cross section $d\sigma_{2\mathrm{tw}}/d\Gamma$, with $d\Gamma = dE_1 d\Omega_1 d\Omega_2$, for the double Compton scattering of a superposition of two equally intense beams of twisted γ-ray photons, of energy $E_0 = 0.4$ MeV, with given OAM difference Δm, scattering from electrons at rest. Results are plotted as a function of the scattering angles θ_2 and ϕ_2 for selected values of Δm and cone opening angle θ_p. Top row: $\Delta m = 0$. Middle row: $\Delta m = 1$. Bottom row: $\Delta m = 2$. For all panels, $E_1 = 50$ keV, $\theta_1 = 35^\circ$, $\phi_1 = 0^\circ$, and phase constant $\delta = 0$. The color-coded scale for all panels displayed at lower right is in units of $\mu b/sr^2$ MeV.

values of the polar angle θ_2 as E_0 increases. Furthermore, the results indicate that the precise dependence of R_z is strongly affected by the value of θ_1 and much less by E_1.

Numerical results for R_x versus the energy of incident twisted photon E_0 are displayed in Fig. 8. The results are shown for selected values of the energy E_1 for $\theta_1 = 35^\circ$ in Fig. 8(a). The results are displayed, in Fig. 8(b), for selected values of θ_1 while $E_1 = 50$ keV. As these results show, the parameter R_x steadily increases with increasing E_0. For certain values of the parameters, such as when $\theta_1 = 35^\circ$, R_x can increase from negative to positive values. For these values, there is an energy $E_0 \approx 0.9$ MeV of the twisted photon around which the dependence of the angular distributions on ϕ_2 is insensitive to changes in the cone opening angle θ_p.

C. Differential cross section for a superposition of twisted photons

The angular distribution of scattered photons for the double Compton scattering of photons prepared in a single pure Bessel state is sensitive to the cone opening angle θ_p but not to the projection of orbital angular momentum m.

We now analyze the double Compton scattering of a photon prepared in a coherent superposition of two twisted Bessel states with equal longitudinal and transverse momenta $\kappa_{p_\parallel}$ and $\kappa_{p_\perp}$, equal helicity Λ, but with two different values of angular momentum projection m_1 and $m_2 > m_1$. Superpositions of twisted beams have been considered in several previous theoretical studies, for example [51,52,55], where it was shown that the angular distributions of the scattered particles depend not on the specific value of m_1 or m_2 individually but instead on the difference $\Delta m = m_2 - m_1$. A superposition of twisted states has also been realized experimentally [56], at least for low-energy photons. A photon prepared in such a superposition is described by the state vector

$$|\gamma\rangle = c_1\,|\kappa_{p_\perp}\kappa_{p_\parallel} m_1 \Lambda\rangle + c_2\,|\kappa_{p_\perp}\kappa_{p_\parallel} m_2 \Lambda\rangle, \qquad (31)$$

where the coefficients fulfill $|c_1|^2 + |c_2|^2 = 1$ and the state $|\gamma\rangle$ is normalized $\langle\gamma|\gamma\rangle = 1$. One suitable choice for the coefficients c_n is $c_1 = 1/\sqrt{2}$ and $c_2 = e^{i\delta}/\sqrt{2}$. These coefficients are of equal modulus and therefore each twisted state in the superposition is weighted equally. This superposition state can therefore be described by the plane-wave decomposition given in Eq. (10) except that the transverse amplitude given by Eq. (12) is replaced by the modified transverse amplitude [55]

$$A_{\kappa_{p_\perp} m_1 m_2}(\vec{p}_{0_\perp}) = \frac{1}{\sqrt{2}}[a_{\kappa_{p_\perp} m_1}(\vec{p}_{0_\perp}) + e^{i\delta} a_{\kappa_{p_\perp} m_2}(\vec{p}_{0_\perp})], \qquad (32)$$

but for which the plane-wave components are no longer distributed uniformly over the azimuthal angle ϕ_p. Consequently, the S matrix for a superposition of Bessel states is constructed

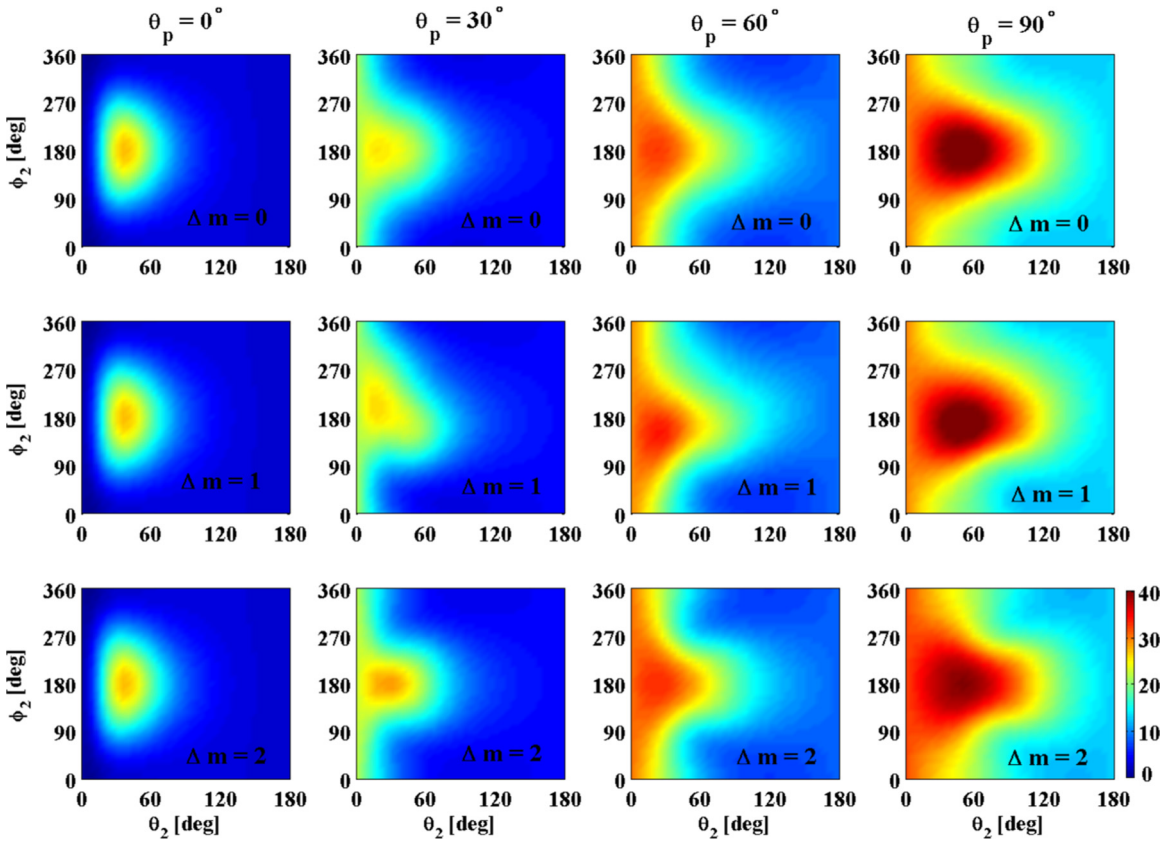

FIG. 10. Differential cross section $d\sigma_{2\mathrm{tw}}/d\Gamma$, with $d\Gamma = dE_1 d\Omega_1 d\Omega_2$ plotted as a function of the scattering angles θ_2 and ϕ_2, for selected values of Δm and cone opening angle θ_p. Top row: $\Delta m = 0$. Middle row: $\Delta m = 1$. Bottom row: $\Delta m = 2$. All other parameters are the same as for Fig. 9, except $\theta_1 = 145^\circ$

as in Eq. (14) but with the transverse amplitude replaced by the modified transverse amplitude. This new amplitude modifies Eq. (15), which relates the differential cross section for a twisted photon to the corresponding plane-wave differential cross section, to the modified form for a superposition of twisted Bessel states [51],

$$\frac{d\sigma_{2\mathrm{tw}}}{d\Gamma} = \frac{d\sigma_{2\mathrm{tw}}}{dE_1 d\Omega_1 d\Omega_2} = \int \frac{d\phi_p}{2\pi} F(\phi_p) \frac{d\sigma_{\mathrm{PW}}(\theta_p,\phi_p)}{dE_1 d\Omega_1 d\Omega_2}, \quad (33)$$

where the azimuthal distribution

$$F(\phi_p) = 1 + \cos\left[\Delta m\left(\phi_p - \frac{\pi}{2}\right) + \delta\right] \quad (34)$$

depends on the difference of the projection numbers, $\Delta m = m_2 - m_1$. As with the calculation of the twisted differential cross section in Eq. (15), the differential cross section for each plane-wave component in Eq. (33) is assumed, in this paper, to be averaged over the helicity components of the initial electron and polarization components of the incident photon and summed over helicity components of the final electron and polarizations of the scattered photons.

The results for $E_0 = 0.4$ MeV, $\theta_1 = 35^\circ$, and $E_1 = 50$ keV are shown in Fig. 9. The top row of panels is for a pure twisted beam, that is, $\Delta m = 0$, and coincides with results presented earlier in Fig. 3, which display reflection symmetry of the angular distributions with respect to the x-z plane. The middle row of panels shows the results with $\Delta m = 1$, and the bottom row of panels shows the results for $\Delta m = 2$. The panels in the first column are the results for $\theta_p = 0^\circ$, coinciding with plane waves, and are clearly independent of Δm.

As indicated in Fig. 9, the effect of the superposition state is to induce deviations in the dependence of the angular distributions on the scattering angle ϕ_2 as compared to pure twisted case $\Delta m = 0$. This azimuthal modulation depends on the value of Δm and on the cone opening angle θ_p. When $\Delta m = 1$, for example, the reflection symmetry with respect to the x-z plane is destroyed. The effect of this superposition is to enhance the angular distribution in the $y < 0$ half space and diminish the distribution in the $y > 0$ half space as compared to the case $\Delta m = 0$. For $\Delta m = 2$, displayed in the bottom row of panels, the distributions become mirror symmetric with respect to the x-z plane again, like the distributions of $\Delta m = 0$, but with additional azimuthal modulation superimposed.

The results for $\theta_1 = 145^\circ$ are shown in Fig. 10. All other parameters are the same as for Fig. 9. The first row of panels is for the pure twisted case $\Delta m = 0$ and corresponds to the angular distributions in Fig. 4. The results clearly show the same trends in the azimuthal modulation of the angular distributions as described for Fig. 9.

For $|\Delta m| > 2$, additional results, not shown in Figs. 9 and 10 but calculated with the same values of parameters, indicate the continuing trend that the angular distributions become asymmetric with respect to the x-z plane for odd Δm, and reflection symmetry is restored for even Δm, with

the number of azimuthal modulations in the distributions increasing with an increase of $|\Delta m|$.

However, as $|\Delta m|$ increases, deviations from the single OAM eigenstate $\Delta m = 0$ remain large only for increasingly large cone opening angles θ_p. Once $\Delta m = 4$, for example, the angular distributions for $\theta_p = 30^\circ$ deviate very little from the corresponding distributions for $\Delta m = 0$ shown in Figs. 9 and 10, but the angular distributions for $\theta_p = 60$ and 90° still show pronounced modulation, although, once $|\Delta m| > 6$, all the angular distributions are nearly indistinguishable from their corresponding distribution for the single OAM eigenstate, $\Delta m = 0$, regardless of the value of θ_p. In light of results reported elsewhere for single Compton scattering of twisted photons [52], these results indicate that the value of the cone opening angle θ_p adjusts the weight of the various nondipole contributions, with higher-order nondipole contributions suppressed for small θ_p.

IV. SUMMARY AND CONCLUSION

In summary, a theoretical study has been performed for the double Compton scattering of γ-ray photons from a Bessel beam on electrons in the rest frame of the electrons. Relativistic quantum electrodynamics has been used to analyze the energy-and-double-angle-differential cross section as a function of the scattering angles and for Bessel beams with different momentum cone opening angles and orbital angular momentum.

The angular distributions are sensitive to the momentum cone opening angle θ_p. The degree of sensitivity depends on the energy E_0 of the initial twisted photon, the scattering angle θ_1, and energy E_1 of the first scattered photon, but not on the value of the OAM projection number m. In particular, for certain combinations of the input parameters, there are energies of the initial twisted photon at and near which certain characteristics of the angular distributions, such as their azimuthal or polar symmetry, are *insensitive* to the cone opening angle.

It was also found that, for incoming photons prepared in a superposition of twisted states, significant differences in the angular distributions occur from the case of an incoming photon prepared in a single twisted state. The changes induced depend on the difference of the OAM projection Δm and on θ_p.

An important feature for the experimental verification of these effects is the availability of twisted photon beams of sufficiently high energy. This requires twisted beams on the order of the electron rest mass energy or higher to render the cross section for double Compton scattering large enough to be optimally observed. The generation of twisted beams at these energies and with large cone opening angles may prove to be experimentally challenging. However, rapid progress has been made to generate beams at ever higher energies, from early beams at low-energy optical frequencies to the recent realization of XUV beams [45]. The recent proposals [47,49,50] to produce twisted photons with energies of $\gtrsim$1 MeV suggest that the necessary photon beams will be available in the near future.

[1] J. D. Jackson, *Classical Electrodynamics*, 3rd ed. (Wiley, New York, 1998).
[2] O. Klein and Y. Nishina, Z. Phys. A **52**, 853 (1929).
[3] A. H. Compton, Phys. Rev. **21**, 483 (1923).
[4] M. Kaku, *Quantum Field Theory: A Modern Introduction* (Oxford University, New York, 1993).
[5] J. Felsteiner and P. Pattison, Nucl. Instrum. Methods **173**, 323 (1980).
[6] E. Lötstedt and U. D. Jentschura, Phys. Rev. Lett. **103**, 110404 (2009).
[7] E. Lötstedt and U. D. Jentschura, Phys. Rev. A **80**, 053419 (2009).
[8] D. Seipt and B. Kämpfer, Phys. Rev. D **85**, 101701 (2012).
[9] F. Mackenroth and A. Di Piazza, Phys. Rev. Lett. **110**, 070402 (2013).
[10] F. Mandl and T. H. R. Skyrme, Proc. R. Soc. A **215**, 497 (1952).
[11] J. M. Jauch and F. Rohrlich, *The Theory of Photons and Electrons*, 2nd ed. (Springer, Heidelberg, 1980).
[12] F. Bell, arXiv:0809.1505.
[13] E. Lötstedt and U. D. Jentschura, Phys. Rev. A **87**, 033401 (2013).
[14] P. E. Cavanagh, Phys. Rev. **87**, 1131 (1952).
[15] M. R. McGie, F. P. Brady, and W. J. Knox, Phys. Rev. **152**, 1190 (1966).
[16] M. R. McGie and F. P. Brady, Phys. Rev. **167**, 1186 (1968).
[17] B. S. Sandhu, R. Dewan, B. Singh, and B. S. Ghumman, Phys. Rev. A **60**, 4600 (1999).
[18] B. S. Sandhu, R. Dewan, M. B. Saddi, B. Singh, and B. S. Ghumman, Nucl. Instrum. Methods Phys. Res. B **168**, 329 (2000).
[19] M. B. Saddi, B. S. Sandhu, and B. Singh, Ann. Nucl. Energy **33**, 271 (2006).
[20] M. B. Saddi, B. Singh, and B. S. Sandhu, Nucl. Instrum. Methods Phys. Res. B **266**, 3309 (2008).
[21] M. B. Saddi, B. Singh, and B. S. Sandhu, Nucl. Technol. **175**, 168 (2011).
[22] L. Allen, M. W. Beijersbergen, R. J. C. Spreeuw, and J. P. Woerdman, Phys. Rev. A **45**, 8185 (1992).
[23] M. W. Beijersbergen, L. Allen, H. E. L. O. van der Veen, and J. P. Woerdman, Opt. Commun. **96**, 123 (1993).
[24] G. Molina-Terriza, J. P. Torres, and L. Torner, Nat. Phys. **3**, 305 (2007).
[25] *The Angular Momentum of Light*, edited by D. L. Andrews and M. Babiker (Cambridge University, Cambridge, England, 2013).
[26] S. M. Barnett and L. Allen, Opt. Commun. **110**, 670 (1994).
[27] L. Allen, M. Padgett, and M. Babiker, *Progress in Optics* (Elsevier, Amsterdam, 1999), Vol. 39, p. 291372.
[28] A. M. Yao and M. J. Padgett, Adv. Opt. Photonics **3**, 161 (2011).
[29] X. Cai, J. Wang, M. J. Strain, B. Johnson-Morris, J. Zhu, M. Sorel, J. L. O'Brien, M. G. Thompson, and S. Yu, Science **338**, 363 (2012).
[30] N. Bozinovic, Y. Yue, Y. Ren, M. Tur, P. Kristensen, H. Huang, A. E. Willner, and S. Ramachandran, Science **340**, 1545 (2013).

[31] H. He, M. E. J. Friese, N. R. Heckenberg, and H. Rubinsztein-Dunlop, Phys. Rev. Lett. **75**, 826 (1995).
[32] M. Padgett and R. Bowman, Nat. Photonics **5**, 343 (2011).
[33] A. Jesacher, S. Fürhapter, S. Bernet, and M. Ritsch-Marte, Phys. Rev. Lett. **94**, 233902 (2005).
[34] J. Verbeeck, H. Tian, and P. Schattschneider, Nature (London) **467**, 301 (2010).
[35] A. Afanasev, C. E. Carlson, and A. Mukherjee, Phys. Rev. A **88**, 033841 (2013).
[36] H. M. Scholz-Marggraf, S. Fritzsche, V. G. Serbo, A. Afanasev, and A. Surzhykov, Phys. Rev. A **90**, 013425 (2014).
[37] A. Surzhykov, D. Seipt, V. G. Serbo, and S. Fritzsche, Phys. Rev. A **91**, 013403 (2015).
[38] A. Picón, J. Mompart, J. R. Vázquez de Aldana, L. Plaja, G. F. Calvo, and L. Roso, Opt. Express **18**, 3660 (2010).
[39] D. Seipt, R. A. Müller, A. Surzhykov, and S. Fritzsche, Phys. Rev. A **94**, 053420 (2016).
[40] J. Arlt, K. Dholakia, L. Allen, and M. J. Padgett, J. Mod. Opt. **45**, 1231 (1998).
[41] A. G. Peele, P. J. McMahon, D. Paterson, C. Q. Tran, A. P. Mancuso, K. A. Nugent, J. P. Hayes, E. Harvey, B. Lai, and I. McNulty, Opt. Lett. **27**, 1752 (2002).
[42] B. Terhalle, A. Langner, B. Päivänranta, V. A. Guzenko, C. David, and Y. Ekinci, Opt. Lett. **36**, 4143 (2011).
[43] G. Gariepy, J. Leach, K. T. Kim, T. J. Hammond, E. Frumker, R. W. Boyd, and P. B. Corkum, Phys. Rev. Lett. **113**, 153901 (2014).
[44] C. Hernández-García, J. San Román, L. Plaja, and A. Picón, New J. Phys. **17**, 093029 (2015).
[45] R. Géneaux, A. Camper, T. Auguste, O. Gobert, J. Caillat, R. Taeib, and T. Ruchon, Nat. Commun. **7**, 12583 (2016).
[46] U. D. Jentschura and V. G. Serbo, Phys. Rev. Lett. **106**, 013001 (2011).
[47] U. D. Jentschura and V. G. Serbo, Eur. Phys. J. C **71**, 1571 (2011).
[48] V. Petrillo, G. Dattoli, I. Drebot, and F. Nguyen, Phys. Rev. Lett. **117**, 123903 (2016).
[49] Y. Taiga, T. Hayakawa, and M. Katoh, arXiv:1608.04894.
[50] C. Liu, B. Shen, X. Zhang, Y. Shi, L. Ji, W. Wang, L. Yi, L. Zhang, T. Xu, Z. Pei, and Z. Xu, Phys. Plasmas **23**, 093120 (2016).
[51] D. Seipt, A. Surzhykov, and S. Fritzsche, Phys. Rev. A **90**, 012118 (2014).
[52] S. Stock, A. Surzhykov, S. Fritzsche, and D. Seipt, Phys. Rev. A **92**, 013401 (2015).
[53] I. P. Ivanov, V. G. Serbo, and V. A. Zaytsev, Phys. Rev. A **93**, 053825 (2016).
[54] M. E. Peskin and D. V. Schroeder, *An Introduction to Quantum Field Theory* (Westview, Boulder, 1995).
[55] I. P. Ivanov, Phys. Rev. D **83**, 093001 (2011).
[56] R. Vasilyeu, A. Dudley, N. Khilo, and A. Forbes, Opt. Express **17**, 23389 (2009).